

Particle acceleration by combined diffusive shock acceleration and downstream multiple magnetic island acceleration

G P Zank^{1,2}, P Hunana¹, P Mostafavi^{1,2}, J A le Roux^{1,2}, Gang Li^{1,2}, G M Webb¹ and O Khabarova³

¹ Center for Space Plasma and Aeronomic Research (CSPAR), University of Alabama in Huntsville, Huntsville, AL 35805, USA

² Department of Space Science, University of Alabama in Huntsville, Huntsville, AL 35805, USA

³ Heliophysical Laboratory, Institute of Terrestrial Magnetism, Ionosphere and Radiowave Propagation RAS (IZMIRAN), Troitsk, Moscow 142190, Russia

E-mail: garyp.zank@gmail.com

Abstract. As a consequence of the evolutionary conditions [28; 29], shock waves can generate high levels of downstream vortical turbulence. Simulations [32–34] and observations [30; 31] support the idea that downstream magnetic islands (also called plasmoids or flux ropes) result from the interaction of shocks with upstream turbulence. Zank et al. [18] speculated that a combination of diffusive shock acceleration (DSA) and downstream reconnection-related effects associated with the dynamical evolution of a “sea of magnetic islands” would result in the energization of charged particles. Here, we utilize the transport theory [18; 19] for charged particles propagating diffusively in a turbulent region filled with contracting and reconnecting plasmoids and small-scale current sheets to investigate a combined DSA and downstream multiple magnetic island charged particle acceleration mechanism. We consider separately the effects of the anti-reconnection electric field that is a consequence of magnetic island merging [17], and magnetic island contraction [14]. For the merging plasmoid reconnection-induced electric field only, we find i) that the particle spectrum is a power law in particle speed, flatter than that derived from conventional DSA theory, and ii) that the solution is constant downstream of the shock. For downstream plasmoid contraction only, we find that i) the accelerated particle spectrum is a power law in particle speed, flatter than that derived from conventional DSA theory; ii) for a given energy, the particle intensity peaks downstream of the shock, and the peak location occurs further downstream of the shock with increasing particle energy, and iii) the particle intensity amplification for a particular particle energy, $f(x, c/c_0)/f(0, c/c_0)$, is not 1, as predicted by DSA theory, but increases with increasing particle energy. These predictions can be tested against observations of electrons and ions accelerated at interplanetary shocks and the heliospheric termination shock.

1. Introduction

Energetic particles are thought to be accelerated at shock waves by a process known as diffusive shock acceleration (DSA). DSA has been invoked to explain energetic particle acceleration throughout the universe, from gradual solar energetic particle events [1–9] to galactic cosmic rays (e.g., [10]). For DSA, the particle intensity at a given energy increases exponentially



ahead of the shock, with a scale length $L^{-1} \simeq U_1/\kappa$, where U_1 is the upstream flow speed and κ is a spatial diffusion coefficient describing the scattering of charged particles in magnetic turbulence. The accelerated particle distribution function at and downstream of the shock is constant spatially and a power law in momentum p^{-w} , where $w = 3r/(r - 1)$ depends only on the shock compression ratio r .

The DSA of electrons is difficult because electrons of moderate energy cannot resonantly scatter of background Alfvénic fluctuations associated with the proton streaming instability at a shock [11]. It is possible that some other mechanism may therefore be responsible for either pre-energizing or fully accelerating electrons in the vicinity of a shock. [12] surveyed proton and electron intensity-time profiles of 168 forward interplanetary shocks observed by the ACE spacecraft between September 1997 and December 2001, finding that there were almost as many events corresponding to classical DSA events as events that had either step-like or irregular post-shock increases in the proton intensity. However, step-like post-shock increases are much more common for electrons (energy range 38 - 53 keV) than protons. [12] conclude that there is a clear trend towards the peak intensities occurring in the downstream region of the shock, confirmed by [13] with a more extended study. Complex magnetic field geometrical effects do not explain the post-shock peaking of the observed electron intensity-time profiles. The frequent observed peaking of proton and electron intensity-time profiles some distance/time behind the shock is quite different from the predictions of DSA.

The acceleration of electrons and ions by magnetic island reconnection-related processes has been proposed by [14–17], and extended by [18; 19]. Reconnection associated with merging and contracting plasmoids or flux ropes can lead to the first-order Fermi energization of electrons and ions of initially moderate energies trapped in the islands. Simulations often reveal the generation of a rather hard power law spectrum in a “sea of magnetic islands” (e.g., [17; 20]). The transport theory developed by [18] and [19] incorporates energy changes to the charged particle distribution function (ions or electrons) by magnetic island contraction and merging. For a fixed steady source of particles injected into a super-Alfvénic flow filled with dynamically interacting magnetic islands, the general (Greens function) solution is a power law-like spectrum with an index that depends on the Alfvén Mach number and the ratio τ_{diff}/τ_c of the charged particle diffusion time scale τ_{diff} and the magnetic island/plasmoid/flux rope contraction time scale τ_c [18] .

In situ evidence that electrons and possibly ions are energized in solar wind regions filled with magnetic islands or plasmoids has emerged in the past few years. The distribution of solar wind small-scale discontinuities has been associated with small-scale magnetic islands or flux ropes [21; 22], and increases in the electron and ion heating and heat flux [23; 24]. Shock waves observed in the vicinity of the heliospheric current sheet appear to exhibit electron heating and energization [25; 26] related to the presence of magnetic islands. Further possible evidence of electron acceleration by magnetic islands may have been found by [27], with superhalo (~ 2 - 20 keV) electrons observed during quiet time periods. Quiet time superhalo electrons were observed i) almost exclusively in the slow solar wind, ii) to be isotropically distributed, and iii) to possess power law spectra in particle speed $c^{-\gamma}$, with $\gamma \in [5, 8.7]$. Nearly half the spectra lie in the interval $\gamma \in [6.5, 7.5]$. We have suggested that charged particles can be accelerated during quiet times in the vicinity of the heliospheric current sheet [18; 26], where a large population of magnetic islands may be expected. Power law distributions for accelerated electrons with spectral indices ranging from ~ 6 - 7 between ~ 0.8 - 2 AU for the simplest case of magnetic island merging can be derived from the theory of [18] (see Figure 6 of [18]). It is possible that the origin of the quiet time electron superhalo spectra observed by [27] may well be due to stochastic particle acceleration by distributed magnetic islands in the neighborhood of the heliospheric current sheet.

The shock evolutionary conditions [28; 29] show that downstream vortical modes are

generated by the transmission of upstream fluctuations through the shock. Observed [30; 31] and simulated [32–34] shock waves generate substantial levels of MHD turbulence, vortices, and structures downstream of shocks. Downstream magnetic islands will contract and merge dynamically as they advect away from the shock. [18] speculated that because shocks typically generate significant levels of vortical turbulence downstream, reconnection associated with plasmoid contraction and merging may be partly responsible for the acceleration of charged particles at collisionless shock waves. This may be particularly important for electrons.

Based primarily on theory and simulations that indicate that shocks generate vortical turbulence, we present a preliminary extension of the basic test particle theory of DSA [35–39] to include particle energization by downstream magnetic field islands. We consider fast mode shocks only and solve two special cases.

2. Coupled DSA and magnetic island acceleration of charged particles

Three processes can increase the energy of test particles interacting with a dynamical “sea” of magnetic islands. (1) As an elongated island contracts, trapped particles experience repeated reflections at either end of the contracting plasmoid. Particles are energized by a first-order Fermi process [14] due to curvature drift in the direction of the induced electric field generated at the strongly curved magnetic field at the endpoints of a contracting flux rope, or in the outflow regions of reconnection sites between merging plasmoids [14; 18; 19; 40; 41]. (2) Depending on whether the magnetic island contraction is compressible or incompressible, the magnetic field strength will either increase or decrease. In the former case, betatron acceleration of the particle will contribute to the energy gain, whereas in the latter case, betatron deceleration will result, both a consequence of charged particle conservation of magnetic moment [18; 19]. The compressible plasmoid contraction case yields a first-order Fermi energization mechanism [18; 19], whereas the incompressible mechanism corresponds to a second-order Fermi energization mechanism [16; 18; 19]. (3) Particles trapped inside an island merger will repeatedly interact with the “anti-reconnection” electric field induced by the merging process [17; 42–45], leading to electron heating and energization. This is a form of direct acceleration by the reconnection-induced electric field component parallel to the magnetic field. Test particle simulations by [17] and [45] concluded that particle acceleration by the induced electric field associated with small-scale magnetic island merging may be the dominant energization process for particles in reconnection layers. However, test particle simulations of electron acceleration in a region of cascading magnetically reconnecting magnetic islands [41] suggest that electron energization is due primarily to magnetic field curvature and gradients, i.e., by either compressible or incompressible magnetic island contraction. These two sets of somewhat contradictory simulations do not make it clear which process is likely to dominate the energization of charged particles in flux rope-related reconnection processes. Accordingly, we retain both mechanisms in our transport theory [18; 19] and explore the effects of both.

2.1. Transport formalism

[18] derived a transport equation for a gyrotropic distribution of particles experiencing pitch-angle scattering and energization via the three reconnection-related processes described above for a super-Alfvénic plasma flow. The gyrophase-averaged or focused transport equation can be simplified further by assuming a nearly isotropic particle distribution [18], yielding an advection-diffusion transport equation that resembles the familiar Parker-Gleeson-Axford cosmic ray transport equation (e.g., [46]). [18] and [19] make the important implicit assumption that the time scale over which the particle distribution is averaged is much longer than the trapping time τ_{trap} for particles trapped in individual plasmoids.

The first-order correct transport equation can be expressed as

$$\begin{aligned} \frac{\partial f}{\partial t} + (U_i + 3|V_E|b_i) \frac{\partial f}{\partial x_i} - \frac{c}{3} \frac{\partial U_i}{\partial x_i} \frac{\partial f}{\partial c} + \frac{1}{c^2} \frac{\partial}{\partial c} \left(\frac{c^3}{3} 2\eta_c f \right) = \frac{\partial}{\partial x_i} \left(K_{ij} \frac{\partial f}{\partial x_j} \right) \\ - c \frac{\partial}{\partial x_i} \left(|V_E|_i \frac{\partial f}{\partial c} \right) - |V_E|_i c \frac{\partial^2 f}{\partial x_i \partial c}, \end{aligned} \quad (1)$$

where $f = f(\mathbf{x}, t, c)$ is the charged particle distribution function in terms of particle position \mathbf{x} , time t , and speed c . \mathbf{U} is the background large-scale plasma flow velocity, $\mathbf{b} \equiv \mathbf{B}/|\mathbf{B}|$ is the unit vector in the direction of the magnetic field, $|V_E| \equiv 1/3q/m\delta E_3\tau_s$ relates the anti-reconnection electric field along the \mathbf{b} direction δE_3 to particle scattering via τ_s , the characteristic pitch-angle scattering time, and q and m are the particle charge and mass respectively ([17; 18; 45] - see also [47]). The term η_c describes the characteristic contraction rate of magnetic islands [16; 18; 19; 40; 41]. The second-order Fermi energization term associated with merging magnetic island line shortening or plasmoid incompressibility [16; 18; 19] enters equation (1) only at the second-order and is therefore neglected here. The term \mathbf{K} describes the spatial diffusion of the nearly isotropic distribution of particles due to pitch-angle scattering.

Three energization terms are present in (1), these being (i) the divergence of the large-scale background flow velocity; (ii) a similar term for magnetic island contraction, and (iii) two mixed derivative terms with coefficient $|V_E|$ that incorporate the anti-reconnection electric field.

The phase space conservation form of the transport equation (1) is given by

$$\frac{\partial f}{\partial t} + \frac{\partial S_i}{\partial x_i} + \frac{1}{c^2} \frac{\partial}{\partial c} (c^2 J_p) = 0, \quad (2)$$

where

$$\mathbf{S} \equiv -\mathbf{K} \cdot \nabla f - \frac{c}{3} \frac{\partial f}{\partial c} (\mathbf{U} - 3|\mathbf{V}_E|),$$

is the energetic particle streaming in space, and

$$J_p \equiv \frac{c}{3} (\mathbf{U} + |\mathbf{V}_E|) \cdot \nabla f + \frac{c}{3} 2\eta_c f,$$

is the streaming in momentum space. This formulation is necessary to determine the energetic particle boundary conditions at a shock wave.

3. DSA at fast-mode shocks with downstream magnetic islands

Since equations (1) and (2) are valid for super-Alfvénic flows, they can be applied to fast-mode shocks. Any upstream perturbation incident on a shock generates vortical fluctuations [28; 48]. [32–34; 49; 50] considered the effect of preexisting, large-scale, broadband turbulent fluctuations on propagating hydromagnetic shock waves, using numerical simulations that solve the 2D MHD equations. Upstream density fluctuations induce rippling of the shock surface that generates vorticity and swirling in the downstream flow, stretching and folding the entrained magnetic field. Their simulations show evidence of magnetic islands in the super-Alfvénic downstream flow. We shall assume that collisionless shock waves generate vortical turbulence that evolves dynamically as it is advected away from the shock. For simplicity, we shall further assume that vortical turbulence can be neglected upstream of the shock.

Assuming a planar shock allows us to use a spatially 1D form of the transport equation (1),

$$\frac{\partial f}{\partial t} + (U + 3|V_E|) \frac{\partial f}{\partial x} - \frac{c}{3} \frac{\partial U}{\partial x} \frac{\partial f}{\partial c} + \frac{1}{c^2} \frac{\partial}{\partial c} \left(\frac{c^3}{3} 2\eta_c f \right) = \frac{\partial}{\partial x} \left(K \frac{\partial f}{\partial x} \right) - 2|V_E|c \frac{\partial^2 f}{\partial x \partial c}, \quad (3)$$

for constant upstream and downstream flow fields, U_1 and U_2 , where 1 denotes upstream and 2 downstream quantities. Upstream of the shock, in the absence of magnetic islands, the steady-state form of equation (3) reduces to

$$U_1 \frac{df}{dx} - \frac{d}{dx} \left(K \frac{df}{dx} \right) = 0,$$

which yields as usual [35]

$$f(x, c) = f_1(c) e^{(U_1/K)x}, \quad x < 0 \quad (4)$$

on assuming, for convenience, that $f(-\infty, c) = 0$. This upstream solution will be used for both cases considered below.

To determine the downstream solution that must be matched to (4), we consider two idealized problems. For the first, we set $\eta_c = 0$ and consider the role of the anti-reconnection electric field term $|V_E|$ exclusively, i.e., magnetic island contraction is neglected. This approach assumes that the energization is due primarily to anti-reconnection electric fields [17; 45]. For the second, we include magnetic island contraction only [41] and neglect the island reconnection-induced electric field contribution, i.e., $|V_E| = 0$. In so doing, we isolate the specific physical effects that each energization mechanism engenders. In both examples, we assume for simplicity that the diffusion coefficient K is constant and equal upstream and downstream of the shock. Changing K from one constant to another upstream and downstream is simple but having a non-constant K renders the problem analytically challenging.

3.1. Role of magnetic island anti-reconnection electric field

On assuming that magnetic island contraction can be neglected ($\eta_c = 0$), the downstream steady-state transport equation is then given by

$$\frac{\partial^2 f}{\partial x^2} - 2 \frac{|V_E|}{K} \frac{\partial^2 f}{\partial x \partial \xi} - \frac{U_2 + 3|V_E|}{K} \frac{\partial f}{\partial x} = 0, \quad (5)$$

where we have introduced the variable $\xi \equiv \ln c/c_0$, and c_0 denotes the lower speed (energy) that is described appropriately by the transport formalism (1). Since $-\infty < \xi < \infty$, $x > 0$, we introduce a Fourier transform in ξ ,

$$\begin{aligned} F(\lambda) &= \frac{1}{\sqrt{2\pi}} \int_{-\infty}^{\infty} e^{i\lambda\xi} f(\xi) d\xi; \\ f(\xi) &= \frac{1}{\sqrt{2\pi}} \int_{-\infty}^{\infty} e^{-i\lambda\xi} F(\lambda) d\lambda, \end{aligned}$$

which transforms (5) to

$$\frac{d^2 F}{dx^2} - \frac{U_2 + 3|V_E| - i2|V_E|}{K} \frac{dF}{dx} = 0. \quad (6)$$

On imposing boundedness as $x \rightarrow \infty$, the solution to (6) is simply

$$F(x, \lambda) = G(\lambda), \quad (7)$$

where $G(\lambda)$ is constant in x and to be determined by the boundary conditions imposed by the conservation form (2). The first boundary condition is simply continuity of the isotropic distribution function $f(x, \xi)$ across the shock, i.e., $[f] = f(0^+) - f(0^-) = 0$, where 0^\pm denotes the value of $f(x, \xi)$ on either side of the shock discontinuity located at $x = 0$. Use of (4) and (7) yields

$$f_1(\xi) = g(\xi), \quad (8)$$

where $g(\xi) = \mathcal{F}^{-1}[G(\lambda)]$ denotes the inverse Fourier transform of $G(\lambda)$. The Fourier transform of the second boundary condition,

$$\left[K \frac{\partial f}{\partial x} + (U - 3|V_E|) \frac{c}{3} \frac{\partial f}{\partial c} \right] = Q\delta(c - c_0), \quad (9)$$

where $Q \equiv \dot{n}/4\pi c_0^2$ (\dot{n} denotes the injection rate of particles into the acceleration process and c_0 is the injected particle speed). Use of (4) and (8) yields

$$G(\lambda) = -\frac{i}{\sqrt{2\pi}} \frac{3\bar{Q}}{U_1 - U_2 + 3|V_E|} \frac{1}{\lambda + i3r/(r-1+3|V_E|/U_2)}, \quad (10)$$

where $r \equiv U_1/U_2$ is the shock compression ratio, $\bar{Q} \equiv \dot{n}/(\sqrt{2\pi}4\pi c_0^3)$. Equation (10) is easily inverted using the residue theorem, yielding the energetic charged particle spectrum at and downstream of the shock as

$$g(\xi) = \frac{3\bar{Q}}{U_1 - U_2 + 3|V_E|} \left(\frac{c}{c_0} \right)^{-3r/(r-1+3|V_E|/U_2)}. \quad (11)$$

To illustrate the role of $|V_E|$, a crude estimate of $|V_E|$ can be derived [18] if we assume that δE_3 can be approximated as $V_A B$, B the local magnetic field, and suppose that the scattering time τ_s is inversely proportional to the gyrofrequency $\Omega \equiv |q|B/m$. Then, $|V_E| = |q||\delta E_3|\tau_s/m \sim (|q|/m)V_A B/\Omega = V_A$, allowing us to express $|V_E|/U_2 \sim M_{A2}^{-1}$, where $M_{A2} \equiv U_2/V_{A2}$ is the downstream Alfvén Mach number. If we adopt the relation $|V_E| \sim V_{A2}$, then

$$\tilde{q} \equiv \frac{3r}{r-1+3|V_E|/U_2} \simeq \frac{3r}{r-1+3M_{A2}^{-1}}. \quad (12)$$

Although offering insight into the meaning of $|V_E|$ and the ratio $U_2/|V_E|$, the relationship $U_2/|V_E| = M_{A2}$ is likely too simplistic, as it relates the parameters $|V_E|$ and the compression ratio r through the downstream Alfvén Mach number, which is not obviously apparent. Unless otherwise indicated, we will continue to regard the parameters $U_2/|V_E|$ and r as independent.

Equations (11) and (12) modify slightly the standard result from DSA for which the spectral index is given by $w = 3r/(r-1)$. The spectral index is harder as a result of additional particle acceleration downstream of the shock via the merging induced magnetic island electric field, although like conventional DSA, the downstream particle intensity for a fixed speed c is spatially constant.

The three panels of Figure 1 show two sets of solutions (11), one assuming that $|V_E|/U_2$ and the compression ratio r are independent, and the second that $|V_E|/U_2 \sim V_{A2}/U_2 = M_{A2}^{-1}$. In the latter case, the efficiency of particle acceleration via downstream reconnection induced electric fields is directly related to the shock strength as measured by M_{A2} . The left panel assumes $U_2/|V_E| = 3$ and r varies between 1.5 and 4, and the middle panel assumes $r = 3.5$ and varies $|V_E|/U_2$. The right panel assumes $|V_E| \sim V_{A2}$. Since $3U_2/|V_E|$ is typically the dominant term in (12), varying r makes little difference to the spectral slope (Figure 1, left). For the same reason, holding r fixed and varying $U_2/|V_E|$ leads to significant changes in the spectral slope of the accelerated particles. Also plotted are power law spectra from standard DSA at shocks with the same compression ratio r . As $U_2/|V_E| \rightarrow \infty$, the solution converges to the standard DSA spectrum. The additional acceleration associated with the anti-reconnection electric field hardens the accelerated spectrum, and weak shocks have harder spectra (because of the reduced escape efficiency due to the smaller downstream Alfvén Mach number) than strong shocks. As the shock strength increases, the spectral index \tilde{q} tends to -4 from above, unlike the standard DSA spectral index that tends to -4 from below.

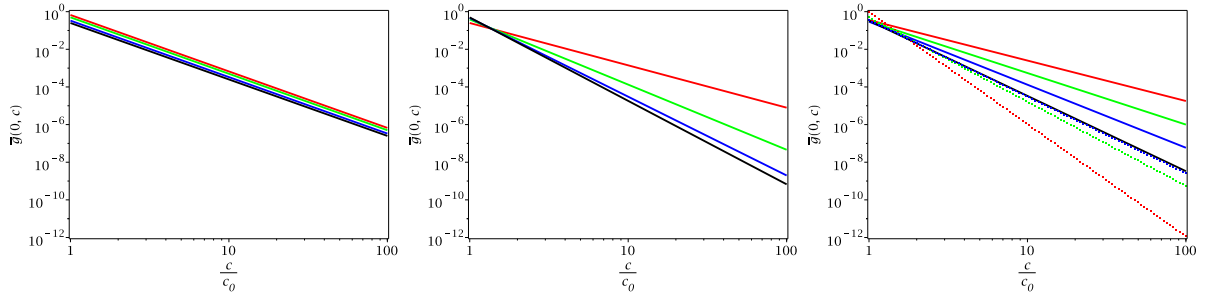


Figure 1. Plot of the charged particle spectrum equation (11), resulting from diffusive shock acceleration in the presence of downstream reconnecting magnetic islands in which the anti-reconnection electric field only is included as an energization term in the transport equation (i.e., the island contraction term $\eta_c = 0$). **Left:** $(|V_E|/U_2)^{-1} \sim 3$ and the shock compression ratio r is varied as $r = 1.5$ (red), $r = 2.0$ (green), $r = 3.0$ (blue), $r = 4.0$ (black). **Middle:** $r = 3.5$ and $(|V_E|/U_2)^{-1} = 1.5$ (red), $(|V_E|/U_2)^{-1} = 5.0$ (green), $(|V_E|/U_2)^{-1} = 20.0$ (blue), $(|V_E|/U_2)^{-1} = 100.0$ (black). **Right:** Here, we assume that $|V_E| \sim V_{A2}$. Three representative solutions are shown for shock compression ratios $r = 2.01$ or $\tilde{q} = 2.15$ (solid red line), $r = 3.03$ or $\tilde{q} = 2.74$ (solid green), $r = 3.80$ or $\tilde{q} = 3.35$ (solid blue). In addition, one solution corresponds to the limit $M_{A2}^2 \rightarrow \infty$, which yields $r = 4.0$ or $\tilde{q} = 4.0$ (solid black line). The dotted lines identify the DSA power law solutions $\propto (c/c_0)^{-w}$, where $w = 3r/(r-1)$. For these cases we have $r = 2.01$ and $w = 5.97$ (dotted red line), $r = 3.03$ and $w = 4.48$ (dotted green), $r = 3.8$ and $w = 4.07$ (dotted blue). The reconnection mediated spectrum becomes steeper with increasing compression ratio r , whereas the DSA spectrum becomes flatter with increasing r .

3.2. Particle acceleration by DSA and magnetic island contraction only

On assuming magnetic island contraction only downstream of the shock, the steady form of the transport equation (3) reduces to

$$\frac{\partial^2 f}{\partial x^2} - \frac{U_2}{K} \frac{\partial f}{\partial x} - \frac{2\eta_c}{3K} \frac{\partial f}{\partial \xi} - \frac{2\eta_c}{K} f = 0, \quad (13)$$

and we assume again that f is bounded as $x \rightarrow \pm\infty$. The Laplace transformed equation (13) is

$$\frac{d^2 \bar{f}}{dx^2} - \frac{U_2}{K} \frac{d\bar{f}}{dx} - \frac{2\eta_c}{3K} (s+3) \bar{f} = 0, \quad (14)$$

and we assume injection of particles at the shock ($x = 0$) only, which implies that $f(x, 0^+) = 0$. Following a procedure similar to that outlined above but using now a Laplace transform approach, the boundary conditions yields the full solution for $x \in \mathcal{R}$ as

$$f(x, \xi) = \begin{cases} g(\xi) e^{(U_1/K)x}, & x < 0; \\ \frac{1}{2\sqrt{\pi}} \sqrt{\frac{2\eta_c}{3K}} x e^{(U_2/2K)x} \int_0^\xi g(\tau) \frac{e^{-s_0(\xi-\tau)} \exp[-\frac{2\eta_c}{3K} x^2/4(\xi-\tau)]}{(\xi-\tau)^{3/2}} d\tau, & x > 0 \end{cases}, \quad (15)$$

The spectrum $g(\xi)$ is given by

$$g(\xi) = \frac{3\bar{Q}}{U_1 - U_2} \frac{1}{\alpha - 3} \left[\left((\bar{q} - 3) - \beta \sqrt{s_0 - 3} \operatorname{erf}(\sqrt{s_0 - 3} \xi^{1/2}) \right) \left(\frac{c}{c_0} \right)^{-3} + \left((\alpha - \bar{q}) + \beta \sqrt{s_0 - \alpha} \operatorname{erf}(\sqrt{s_0 - \alpha} \xi^{1/2}) \right) \left(\frac{c}{c_0} \right)^{-\alpha} \right], \quad (16)$$

where

$$\begin{aligned}\bar{q} &= \frac{3}{2} \frac{2U_1 - U_2}{U_1 - U_2} = \frac{3}{2} \frac{2r - 1}{r - 1}, \quad r = \frac{U_1}{U_2}; \\ \beta &\equiv \frac{\sqrt{6\eta_c K}}{U_1 - U_2} = \frac{\sqrt{6\tau_{diff}/\tau_c}}{r - 1}; \\ \alpha &= \frac{3}{r - 1} \left(r - 2 \frac{\tau_{diff}/\tau_c}{r - 1} \right); \\ s_0 &\equiv 3 \left(1 + \frac{U_2^2/K}{8\eta_c} \right) = 3 \left(1 + \frac{\tau_c}{8\tau_{diff}} \right).\end{aligned}$$

Two characteristic time scales enter (15) and (16), these being the diffusion time scale $\tau_{diff} \equiv K/U_2^2$ and the plasmoid contraction time scale $\tau_c \equiv \eta_c^{-1}$. \bar{Q} is defined as before.

Unlike the standard DSA solution, the downstream contracting magnetic island solution (15) is not constant and instead will continue to increase for a given energy, eventually peaking and then decaying when the e^{-x^2} term dominates. The particle intensity will peak further from the shock with increasing particle energy since there will be more time for particles to experience acceleration by the contracting plasmoids. This effect will eventually be limited by the decay of the post-shock turbulence, for which we have not accounted in our simple model.

Normalized spectra $\bar{g}(c/c_0)$ for the plasmoid contraction-only case for compression ratios $r = 3$ are shown in the top left panel of Figure 2, and the ratio τ_{diff}/τ_c is varied between 0.1 and 5. The spectra are slightly concave at low energies but harden quite significantly at high energies. The solutions are essentially power laws in particle speed, with the hardest spectra corresponding to $\tau_{diff}/\tau_c > 1$. Overplotted is the standard DSA spectrum predicted for a shock with compression ratio 3. The contracting magnetic island spectra are harder and, as $\tau_{diff}/\tau_c \rightarrow 0$, approach the DSA solution from above. The combination of classical DSA and particle acceleration by plasmoid contraction (only) produces power law spectra with indices harder than predicted by DSA alone. Shown in the top right panel of Figure 2 are plots of the DSA-plasmoid contraction-only spectra (normalized) at different distances downstream of the shock. The ratio $\tau_{diff}/\tau_c = 0.5$. For small values of τ_{diff}/τ_c , the spectrum does not change much as the distance from the shock increases, nor does the spectrum change much when close to the shock (within a few diffusion scale lengths downstream of the shock) regardless of the size of τ_{diff}/τ_c . However, as the contraction rate η_c increases relative to the particle diffusion time, the accelerated particle spectrum changes quite markedly with increasing distance from the shock. This is due to the greater gain in energy that a particle experiences as magnetic islands are convected away from the shock. In Figure 2, bottom left, we hold the particle energy fixed and plot the particle intensity profile as a function of distance for $\tau_{diff}/\tau_c = 0.1 - 5$ and compression ratio $r = 3$. All intensity profiles exhibit the exponential increase in particle intensity ahead of the shock (located at $x = 0$), which connects to a downstream solution that continues to increase with increasing distance from the shock. The intensity profile eventually peaks, after which it decays smoothly to zero. The color refers to various choices of τ_{diff}/τ_c . The peak of the intensity profile is located at an increasing distance from the shock as the particle energy increases. The cyan curve shows that the solution converges to the DSA solution when τ_{diff}/τ_c becomes very small i.e., as $\eta_c \rightarrow 0$, the downstream solution is approximately constant with increasing heliocentric distance.

Two important predictions for coupled DSA-reconnection particle acceleration emerge that distinguish this process from the conventional DSA model. These are that the particle intensity peaks downstream of the shock and that the peak occurs further downstream of the shock with increasing charged particle energy. To illustrate this prediction, we plot the spatial profile in the bottom right panel of Figure 2 for magnetic island contraction only, using fixed values of

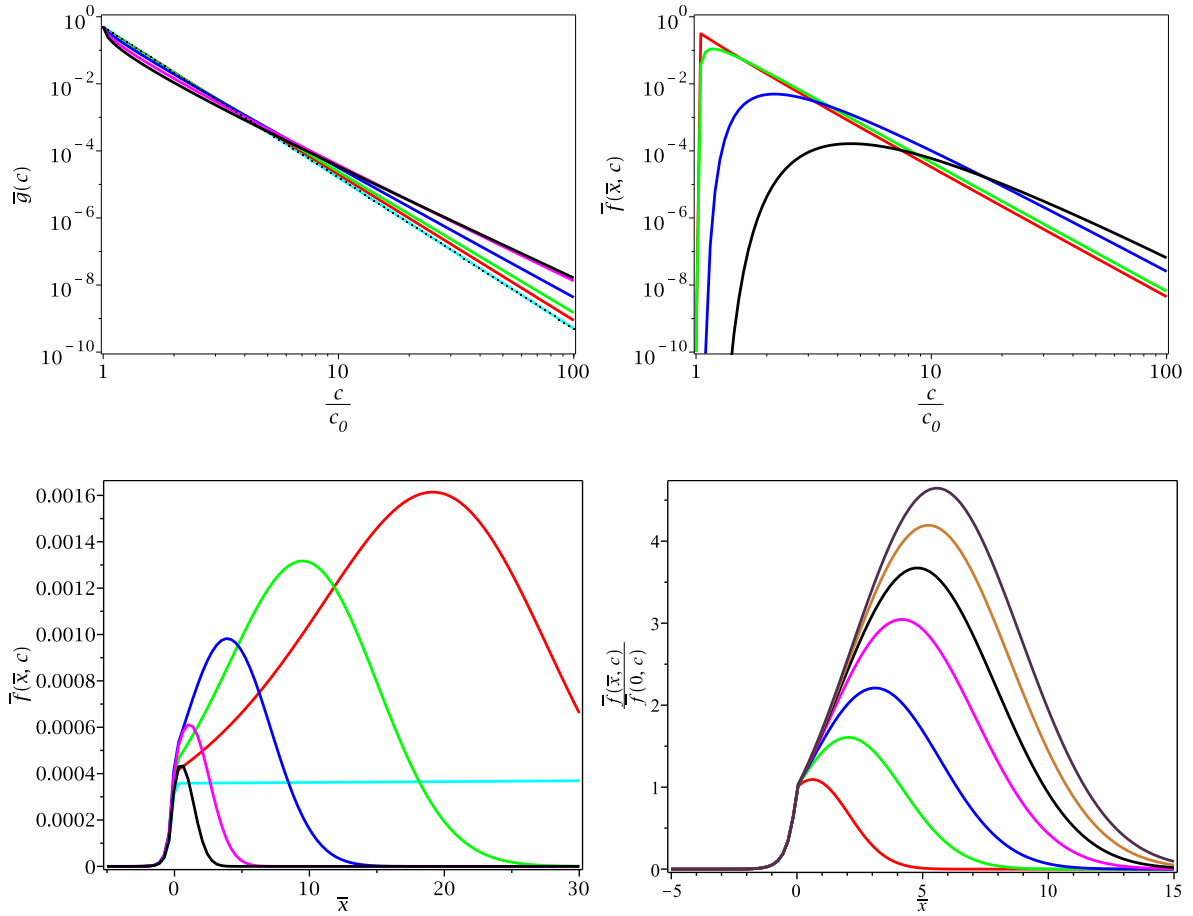


Figure 2. Top Left: Normalized energetic particle spectrum $\bar{g}(c/c_0)$, equation (16), for a compression ratio $r = 3$ in the limiting case of magnetic island contraction only. The colored curves correspond to assumed values of $\tau_{diff}/\tau_c = 0.001$ (cyan line), $\tau_{diff}/\tau_c = 0.1$ (red line), $\tau_{diff}/\tau_c = 0.2$ (green line), $\tau_{diff}/\tau_c = 0.5$ (blue line), $\tau_{diff}/\tau_c = 2.0$ (magenta line), $\tau_{diff}/\tau_c = 5.0$ (black line). The dotted black lines correspond to the DSA power laws $\propto (c/c_0)^{-3r/(r-1)}$ ($r = 3$). As $\tau_{diff}/\tau_c \rightarrow 0$ the spectra converge to the DSA spectrum and with increasing values of τ_{diff}/τ_c , the spectra flatten. **Top Right:** Plots of the normalized accelerated particle spectra downstream of the shock i.e., the solution (15) $\bar{f}(\bar{x} = \text{const.}, c)$ at different normalized distances $\bar{x} = 0.1$ (red line), $\bar{x} = 1.0$ (green line), $\bar{x} = 5.0$ (blue line), $\bar{x} = 10.0$ (black line). A compression ratio $r = 3$ is assumed and $\tau_{diff}/\tau_c = 0.5$. **Bottom Left:** Normalized particle intensity plot for a fixed energy $c/c_0 = 5$ as function of position. Here $\tau_{diff}/\tau_c = 0.001$ (cyan line), $\tau_{diff}/\tau_c = 0.1$ (red line), $\tau_{diff}/\tau_c = 0.2$ (green line), $\tau_{diff}/\tau_c = 0.5$ (blue line), $\tau_{diff}/\tau_c = 2.0$ (magenta line), $\tau_{diff}/\tau_c = 5.0$ (black line). The cyan line corresponds to a solution that is very close to the DSA limit and so remains almost constant downstream of the shock with increasing distance. A compression ratio $r = 3$ is assumed. **Bottom Right:** Particle intensity as a function of position with particle intensities normalized to the value at the shock $\bar{f}(0, c/c_0)$, assuming a ratio $\tau_{diff}/\tau_c = 1.01$. Each colored curve corresponds to a particular normalized (square root of the) energy c/c_0 : $c/c_0 = 2$ (red line), $c/c_0 = 5$ (green line), $c/c_0 = 10$ (blue line), $c/c_0 = 20$ (magenta line), $c/c_0 = 30$ (black line), $c/c_0 = 40$ (gold line), $c/c_0 = 50$ (violet line). $r = 3$.

τ_{diff}/τ_c at different energies. We normalize the plots to the value of the intensity $f(0, c/c_0)$ as measured at the shock, so the figures show an amplification factor relative to the value at the shock. Conventional DSA predicts that the particle intensity downstream of the shock is constant as a function of distance and, when normalized to the intensity $f(0, c/c_0)$, the intensity is 1 for all energies. Contrast this with the curves illustrated in the bottom right panel of Figure 2. Each of the colored curves in the panels corresponds to a particular normalized (square root of the) energy c/c_0 , from $c/c_0 = 2$ (red) to 50 (black). The lowest energies peak close to the shock (located at $x = 0$) and have the lowest amplification factor and higher energies peak further from the shock and have a larger amplification factor. The distance of the particle intensity peak from the shock front is ordered by energy, with the higher energies peaking systematically further from the shock. Similarly, the amplification factor is ordered by energy, with the higher energies having the larger amplification factor. Depending on the assumed value of τ_{diff}/τ_c , the amplification of the particle intensity downstream of the shock can be substantial. As τ_{diff}/τ_c decreases, although the amplification factor increases, the peak location moves further from the shock so that the solution gradually converges towards the DSA limit of no amplification behind the shock.

4. Conclusions

Zank et al. [18] speculated that because shock waves typically generate vortical turbulence, particle acceleration at shocks may be due to a combination of DSA and downstream reconnection processes associated with the dynamical interaction of magnetic islands. We present a simple test particle model, based on the charged particle transport theory developed by [18] and [19], that describes the coupled and simultaneous acceleration of particles at both a shock and downstream interacting merging and contracting magnetic islands.

The transport equation and appropriate boundary conditions for charged particles interacting with a collisionless fast-mode shock and downstream magnetic island turbulence are solved for two cases. Considering the merging plasmoid reconnection-induced electric field only, we find i) that the particle spectrum is a power law in particle speed with an index that depends on the shock compression ratio r and the parameter $U_2/|V_E|$; and ii) that the solution is constant downstream of the shock. The accelerated particle spectrum is flatter than that derived from conventional DSA theory. In the case that only plasmoid contraction is considered, we find that i) the accelerated particle spectrum is a power law in particle speed with an index that depends on the shock compression ratio r and the ratio of the diffusion and the contraction time scales τ_{diff}/τ_c ; ii) the plasmoid contraction-only spectrum is harder than the corresponding DSA spectrum to which it converges as $\tau_{diff}/\tau_c \rightarrow 0$; iii) for a given energy, the particle intensity peaks downstream of the shock, and the peak location occurs further downstream of the shock with increasing particle energy, and iv) the particle intensity amplification for a particular particle energy, $f(x, c/c_0)/f(0, c/c_0)$, is not 1, as predicted by DSA theory, but increases with increasing particle energy.

These two sets of predictions can be tested against observations of electrons and ions accelerated at interplanetary shocks and the heliospheric termination shock.

Acknowledgments

We acknowledge the partial support of NASA grants NNX08AJ33G, Subaward 37102-2, NNX09AG70G, NNX09AG63G, NNX09AJ79G, NNG05EC85C, Subcontract A991132BT, NNX09AP74A, NNX10AE46G, NNX09AW45G, NNX14AF43G, NNN12AA012, NNX15AI65G, and NSF grant ATM-0904007. OK was supported by RFBR grant no. 14-02-00769.

References

- [1] Zank G P, Rice W K M and Wu C C 2000 *J. Geophys. Res.* **105** 25079–25096

- [2] Zank G P, Li G and Verkhoglyadova O 2007 *Space Sci. Rev.* **130** 255–272
- [3] Li G, Zank G P and Rice W K M 2003 *J. Geophys. Res.* **108** 1082–+
- [4] Rice W K M, Zank G P and Li G 2003 *J. Geophys. Res.* **108** 1369–+
- [5] Verkhoglyadova O P, Li G, Zank G P, Hu Q, Cohen C M S, Mewaldt R A, Mason G M, Haggerty D K, von Rosenvinge T T and Looper M D 2010 *Journal of Geophysical Research (Space Physics)* **115** A12103
- [6] Verkhoglyadova O P, Li G, Ao X and Zank G P 2012 *Ap. J.* **757** 75
- [7] Verkhoglyadova O P, Zank G P and Li G 2015 *Phys. Rep.* **557** 1–23
- [8] Reames D V 1999 *Space Sci. Rev.* **90** 413–491
- [9] Reames D V 2013 *Space Sci. Rev.* **175** 53–92 (*Preprint* 1306.3608)
- [10] Axford W I 1981 *International Cosmic Ray Conference* **12** 155–203
- [11] Lee M A 1983 *J. Geophys. Res.* **88** 6109–6119
- [12] Lario D, Ho G C, Decker R B, Roelof E C, Desai M I and Smith C W 2003 *Solar Wind Ten (American Institute of Physics Conference Series vol 679)* ed Velli M, Bruno R, Malara F and Bucci B pp 640–643
- [13] Ho G C, Lario D, Decker R B, Smith C W and Hu Q 2008 *American Institute of Physics Conference Series (American Institute of Physics Conference Series vol 1039)* ed Li G, Hu Q, Verkhoglyadova O, Zank G P, Lin R P and Luhmann J pp 184–189
- [14] Drake J F, Swisdak M, Che H and Shay M A 2006 *Nature* **443** 553–556
- [15] Drake J F, Swisdak M, Schoeffler K M, Rogers B N and Kobayashi S 2006 *Geophys. Res. Lett.* **33** L13105
- [16] Drake J F, Swisdak M and Fermo R 2013 *Ap. J. Lett.* **763** L5 (*Preprint* 1210.4830)
- [17] Oka M, Phan T D, Krucker S, Fujimoto M and Shinohara I 2010 *Ap. J.* **714** 915–926 (*Preprint* 1004.1154)
- [18] Zank G P, le Roux J A, Webb G M, Dosch A and Khabarova O 2014 *Ap. J.* **797** 28
- [19] le Roux J A, Zank G P, Webb G M and Khabarova O 2015 *Ap. J.* **801** 112
- [20] Guo F, Liu Y H, Daughton W and Li H 2015 *ArXiv e-prints (Preprint* 1504.02193)
- [21] Greco A, Matthaeus W H, Servidio S, Chuychai P and Dmitruk P 2009 *Ap. J. Lett.* **691** L111–L114
- [22] Greco A, Matthaeus W H, Servidio S and Dmitruk P 2009 *Phys. Rev. E* **80** 046401
- [23] Osman K T, Matthaeus W H, Greco A and Servidio S 2011 *Ap. J. Lett.* **727** L11
- [24] Chasapis A, Retinò A, Sahraoui F, Vaivads A, Khotyaintsev Y V, Sundkvist D, Greco A, Sorriso-Valvo L and Canu P 2015 *Ap. J. Lett.* **804** L1
- [25] Tessein J A, Matthaeus W H, Wan M, Osman K T, Ruffolo D and Giacalone J 2013 *Ap. J. Lett.* **776** L8
- [26] Khabarova O, Zank G P, Li G, le Roux J A, Webb G M, Dosch A and Malandraki O E 2015 *Ap. J.* **808** 24 (*Preprint* 1504.06616)
- [27] Wang L, Lin R P, Salem C, Pulupa M, Larson D E, Yoon P H and Luhmann J G 2012 *Ap. J. Lett.* **753** L23
- [28] McKenzie J F and Westphal K O 1968 *Physics of Fluids* **11** 2350–2362
- [29] Westphal K O and McKenzie J F 1969 *Physics of Fluids* **12** 1228–1236
- [30] Hu Q, Ao X, Peltzer R and Zank G P 2012 *American Institute of Physics Conference Series (American Institute of Physics Conference Series vol 1500)* ed Hu Q, Li G, Zank G P, Ao X, Verkhoglyadova O and Adams J H pp 192–197

- [31] Hu Q, Zank G P, Li G and Ao X 2013 *American Institute of Physics Conference Series* (*American Institute of Physics Conference Series* vol 1539) ed Zank G P, Borovsky J, Bruno R, Cirtain J, Cranmer S, Elliott H, Giacalone J, Gonzalez W, Li G, Marsch E, Moebius E, Pogorelov N, Spann J and Verkhoglyadova O pp 175–178
- [32] Giacalone J and Jokipii J R 2007 *Ap. J. Lett.* **663** L41–L44
- [33] Lu Q, Hu Q and Zank G P 2009 *Ap. J.* **706** 687–692
- [34] Guo F, Li S, Li H, Giacalone J, Jokipii J R and Li D 2012 *Ap. J.* **747** 98 (*Preprint* 1112.6373)
- [35] Axford W I, Leer E and Skadron G 1977 *International Cosmic Ray Conference* **11** 132–137
- [36] Krymskii G F 1977 *Akademiia Nauk SSSR Doklady* **234** 1306–1308
- [37] Bell A R 1978 *MNRAS* **182** 147–156
- [38] Bell A R 1978 *MNRAS* **182** 443–455
- [39] Blandford R D and Ostriker J P 1978 *Ap. J. Lett.* **221** L29–L32
- [40] Bian N H and Kontar E P 2013 *Physical Review Letters* **110** 151101 (*Preprint* 1302.6090)
- [41] Zhou X, Büchner J, Barta M, Gan W and Liu S 2015 *ArXiv e-prints* (*Preprint* 1504.06486)
- [42] Egedal J, Fox W, Katz N, Porkolab M, Øieroset M, Lin R P, Daughton W and Drake J F 2008 *Journal of Geophysical Research (Space Physics)* **113** A12207
- [43] Pritchett P L 2008 *Physics of Plasmas* **15** 102105
- [44] Tanaka K G, Yumura T, Fujimoto M, Shinohara I, Badman S V and Grocott A 2010 *Physics of Plasmas* **17** 102902
- [45] Le A, Karimabadi H, Egedal J, Roytershteyn V and Daughton W 2012 *Physics of Plasmas* **19** 072120
- [46] Zank G P 2014 *Transport Processes in Space Physics and Astrophysics, Lecture Notes in Physics, Berlin Springer Verlag* vol 877 (Springer New York Heidelberg Dordrecht London)
- [47] le Roux J A, Zank G P and Matthaeus W H 2002 *Journal of Geophysical Research (Space Physics)* **107** 1138
- [48] McKenzie J F and Westphal K O 1969 *Planet. Space Sci.* **17** 1029–1037
- [49] Mizuno Y, Pohl M, Niemiec J, Zhang B, Nishikawa K I and Hardee P E 2011 *Ap. J.* **726** 62 (*Preprint* 1011.2171)
- [50] Fraschetti F 2013 *Ap. J.* **770** 84 (*Preprint* 1304.4956)